Geophysical Research Letters

A Dynamic Model of Mercury's Magnetospheric Magnetic Field

Haje Korth[1] (iD), Catherine L. Johnson[2,3], Lydia Philpott[2] (iD), Nikolai A. Tsyganenko[4] (iD), and Brian J. Anderson[1] (iD)

[1]The Johns Hopkins University Applied Physics Laboratory, Laurel, MD, USA, [2]Department of Earth, Ocean and Atmospheric Sciences, University of British Columbia, Vancouver, British Columbia, Canada, [3]Planetary Science Institute, Tucson, AZ, USA, [4]Institute and Faculty of Physics, Saint Petersburg State University, Saint Petersburg, Russia

Abstract Mercury's solar wind and interplanetary magnetic field environment is highly dynamic, and variations in these external conditions directly control the current systems and magnetic fields inside the planetary magnetosphere. We update our previous static model of Mercury's magnetic field by incorporating variations in the magnetospheric current systems, parameterized as functions of Mercury's heliocentric distance and magnetic activity. The new, dynamic model reproduces the location of the magnetopause current system as a function of systematic pressure variations encountered during Mercury's eccentric orbit, as well as the increase in the cross-tail current intensity with increasing magnetic activity. Despite the enhancements in the external field parameterization, the residuals between the observed and modeled magnetic field inside the magnetosphere indicate that the dynamic model achieves only a modest overall improvement over the previous static model. The spatial distribution of the residuals in the magnetic field components shows substantial improvement of the model accuracy near the dayside magnetopause. Elsewhere, the large-scale distribution of the residuals is similar to those of the static model. This result implies either that magnetic activity varies much faster than can be determined from the spacecraft's passage through the magnetosphere or that the residual fields are due to additional external current systems not represented in the model or both. Birkeland currents flowing along magnetic field lines between the magnetosphere and planetary high-latitude regions have been identified as one such contribution.

1. Introduction

The solar wind and interplanetary magnetic field (IMF) in the inner heliosphere are inherently dynamic and govern the magnetic field in Mercury's magnetosphere to a substantial degree (Slavin et al., 2008, 2009, 2012; Slavin, Lepping, et al., 2010). The solar wind pressure balances the magnetic pressure of the planetary field at the magnetopause (Spreiter et al., 1966), and variations thereof affect the location of this boundary (Johnson et al., 2016; Winslow et al., 2013), on which currents flow to shield the planetary magnetic field from the solar wind environment (Chapman & Ferraro, 1931). In addition, the IMF magnitude and direction control the rate of reconnection between antiparallel components of the interplanetary and planetary magnetic field lines at Earth's dayside magnetopause (Sonnerup, 1974). At Mercury, enhanced reconnection has been observed to result in extreme loading and unloading of magnetic flux in the magnetotail (Slavin, Anderson, et al., 2010). However, the reconnection rate was found to vary inversely with the plasma β, the ratio of thermal pressure to magnetic pressure, in the magnetosheath, while found to be independent of the magnetic shear angle (DiBraccio et al., 2013). Variations in the solar wind electric field tapped in the reconnection process modulate the magnetospheric convection cycle from the dayside reconnection site over the polar cap to the cross-tail current sheet (Dungey, 1963) and affect the intensity of the associated magnetotail current that flows from dawn to dusk in the central magnetosphere and closes via the magnetopause. The magnetospheric current systems generate an external magnetic field, the magnitude of which exceeds Mercury's small dynamo field (Anderson et al., 2012) in much of the magnetosphere (Korth et al., 2004), so that the highly variable solar wind conditions in the inner heliosphere (Korth et al., 2010) produce an extremely dynamic magnetosphere.

Mercury's average external magnetic field attributed to magnetospheric currents system was modeled by Korth et al. (2015) using observations acquired by the magnetometer on the MErcury Surface, Space ENvironment, GEochemistry, and Ranging (MESSENGER) spacecraft (Solomon et al., 2001) over seven Mercury years (24 March 2011 to 28 November 2012). The magnetic residuals of the observations with

respect to the average magnetic field model showed a systematic dependence on magnetic disturbance as defined by an index developed by Anderson et al. (2013). This index was computed from the variability of the magnetic field in three distinct, approximately logarithmically spaced period bands spanning 0.1 s to 300 s to capture magnetospheric activity on different timescales and quantify the level of disturbance unbiased with respect to orbit geometry and heliocentric distance in the range from 0 (*quiet*) to 100 (*highly disturbed*). With respect to the disturbance index, the magnitude of the magnetic residuals was found to increase for enhanced magnetic activity (Korth et al., 2015), a correlation that is consistent with the assumption that the magnetospheric current systems, and thus the external magnetic field, are directly controlled by the solar wind conditions. In addition, the residuals were especially large in regions where substantial variability of the field is expected, for example, near the magnetopause. However, the dependence of the external field on magnetic activity could not be evaluated quantitatively because the spatial distribution of the magnetic field data was too sparse when the data set was subdivided into ranges of magnetic activity. A dynamic magnetic field model could thus not be developed initially.

A major problem in the construction of a dynamic magnetic field model was that solar wind data upstream of Mercury were not available during the MESSENGER mission. For models of Earth's magnetosphere, such observations are commonly used to sort magnetospheric data according to the solar wind conditions under which they were acquired. While MESSENGER traversed the solar wind during sections of every orbit, these observations are essentially uncorrelated with those obtained in the adjacent magnetosphere transits because of the short, ~2 min Dungey cycle time (Slavin et al., 2009). Any assessment of the dynamic state of the system must therefore be inferred directly from the observations within the magnetosphere. The magnetic disturbance index by Anderson et al. (2013) was derived based on this understanding and provides a quantitative measure for the level of activity for magnetospheric studies.

After orbiting Mercury for more than 4 Earth years (>16 Mercury years) while observing the magnetic field nearly continuously and repeatedly over a wide range of solar wind and IMF conditions, MESSENGER has completed its mission. The acquired magnetic field observations sampled a substantial fraction of the solar cycle and provided for repeated coverage of the heliocentric distance range traversed by Mercury's orbit around the Sun and in solar local time so that there are now sufficient data to evaluate the dependence of Mercury's external magnetic field on magnetic activity and to capture the result in a new dynamic magnetospheric model. We present here the first dynamic model of Mercury's magnetospheric magnetic field with dependence on magnetic activity. The new model, termed KT17, uses the same structure and mathematical framework as the KT14 model (Korth et al., 2015) but includes variable parameterizations for the magnetopause standoff distance and for the magnetotail current intensity. The analysis of the additional dependencies is presented in section 2, and the results are discussed and summarized in section 3. The reference implementation of the model in FORTRAN programming language is included in the supporting information.

2. Dependence of Model Parameters on Magnetic Activity

The solar wind dynamic pressure, p_{ram}, balances the magnetic pressure, $p_B = \frac{B^2}{2\mu_0}$, of the planetary field at the magnetopause so that temporal variations in p_{ram} affect the location of the magnetopause. The standoff distance, R_{SS}, of Mercury's magnetopause at the subsolar point further depends on the relative effects of solar wind pressure, induction in the interior, and magnetic reconnection at the magnetopause. When both solar wind pressure and magnetopause reconnection are enhanced, such as during coronal mass ejections and high-speed streams, R_{SS} scales to first order proportional to $p_{ram}^{-1/6}$ (Slavin et al., 2014; Winslow et al., 2013), although magnetic fields induced in the planet's interior strengthen the planetary dipole moment of 190 nT R_M^3 by about 5%, and the effect on the pressure balance lowers the exponent somewhat (Johnson et al., 2016). The effects of induction may be further enhanced for elevated solar wind pressure without increased magnetopause reconnection (Slavin et al., 2014), while strong reconnection in absence of enhanced p_{ram} erodes the magnetopause by transfer of magnetic flux from the dayside to the magnetotail and reduces induction (Slavin & Holzer, 1979). On the other hand, the magnetosphere flaring was found to be invariable with respect to p_{ram} (Winslow et al., 2013). To determine the dependence of R_{SS} on magnetic activity, we apply the approach of Johnson et al. (2016) to observations spanning the period from Mercury orbit insertion on 24 March 2011 to the end of the MESSENGER mission on 30 April 2015. Briefly, for each orbit, the inbound and outbound magnetopause crossing locations in Mercury solar magnetospheric

Table 1
Model Parameters and Residuals Sorted by Magnetic Disturbance

| Disturbance index	Number orbits	r_h (AU)	R_{SS} (R_M)	$f = R_{SS}\, r_h^{-1/3}$	t_1	t_2	RMS residual (nT)
0–20	809	0.399	1.512	2.0531	6.74	1.69	18.5
20–40	808	0.397	1.448	1.9702	7.30	1.92	20.4
40–60	808	0.397	1.413	1.9224	7.52	2.05	22.5
60–80	809	0.393	1.378	1.8822	7.92	2.25	25.2
80–97	687	0.389	1.327	1.8180	8.72	2.40	34.9
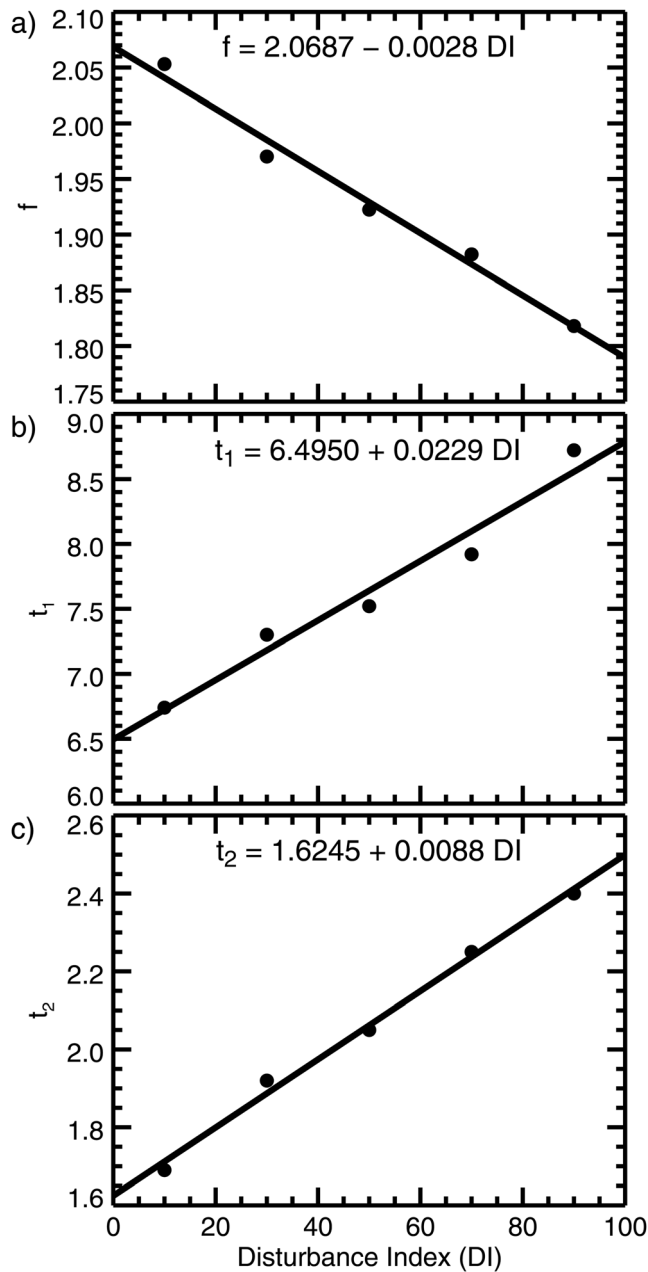
Figure 1. Dependence on the magnetic disturbance index of (a) the magnetopause scale factor, $f = R_{SS}\, r_h^{-1/3}$; (b) disk current amplitude parameter, t_1; and (c) sheet current amplitude parameter, t_2. Linear fits to the data are shown at the top of each panel and are represented by black lines.

(MSM) coordinates corrected for aberration of the magnetotail resulting from Mercury's orbital velocity were identified, and a magnetopause with the functional form of Shue et al. (1997) was fit to these locations to yield R_{SS}. The R_{SS} values were then sorted into 20%-wide bins of the magnetic disturbance index (Anderson et al., 2013). The average R_{SS}, as well as Mercury's average heliocentric distance of the observations, r_h, was computed for each magnetic disturbance bin, and, ignoring small induction effects, the factor $f = R_{SS}\, r_h^{-1/3}$ was calculated, which is the coefficient of proportionality between $r_h^{1/3}$ and the subsolar distance R_{SS}. We excluded orbits associated with the top three percentile of the magnetic disturbance index because these conditions, typically associated with coronal mass ejections, lead to variable (often higher) flaring of the magnetopause, and such deformations of the magnetopause are not considered in the fitting of the magnetopause shape. The bin averages of R_{SS} and f are listed in Table 1, and the linear fit to the f values as function of the magnetic disturbance index is shown in Figure 1a. The results demonstrate that the magnetopause standoff distance decreases with increasing magnetic activity as is expected if the increased magnetic activity is associated with higher solar wind dynamic pressure (Winslow et al., 2013) and enhanced dayside magnetic reconnection (Slavin et al., 2014).

An increase in magnetic activity also leads to enhanced reconnection at the dayside magnetopause. The newly opened magnetic field lines are swept in antisunward direction by the solar wind, reconnect again in the central magnetotail to form closed field lines, and subsequently convect back toward the dayside as the magnetic tension relaxes. Associated with this circulation of magnetic flux is an electric current that flows in the central magnetotail from dawn to dusk to form the cross-tail current sheet. The cross-tail current generates an external magnetic field, which was modeled as a superposition of magnetic fields $\mathbf{B}_d$ and $\mathbf{B}_s$ generated by a disk and a sheet current, respectively. These contributions and that of the internal field, $\mathbf{B}_{int}$, were individually shielded by magnetic fields, $\mathbf{B}_{cf}$, generated at the magnetopause, and summed to yield the total model field (Korth et al., 2015):

$$\mathbf{B}_m = \left(\mathbf{B}_{int} + \mathbf{B}_{cf,int}\right) + t_1 \left(\mathbf{B}_d + \mathbf{B}_{cf,d}\right) + t_2 \left(\mathbf{B}_s + \mathbf{B}_{cf,s}\right). \tag{1}$$

The current intensities are represented by two dimensionless parameters, t_1 for the disk current and t_2 for the sheet current, and their magnitudes were obtained by fitting the magnetic field produced by these currents to the observations in a least squares sense. To determine variations in the cross-tail current intensity with magnetic activity, 1 min averages of magnetic field observations acquired within the magnetosphere between 24 March 2011 and 30 April 2015 were sorted into bins of the magnetic
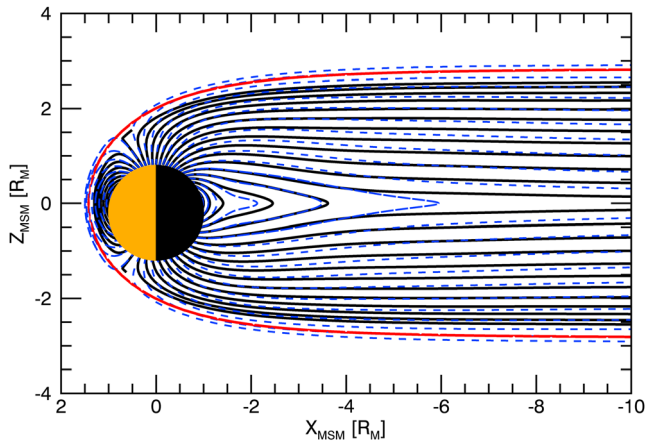
Figure 2. Model magnetic field lines in the noon-midnight plane of the MSM coordinate system for the disturbance indices 95% (black lines) and 5% (blue dashed lines). The average magnetopause location for a disturbance index of 50% is represented by the red line.

disturbance index each again 20% wide. The data in each bin were then fit by minimizing the root-mean-square (RMS) residual of the model field, $\mathbf{B}_m$, with respect to the MESSENGER observations, $\mathbf{B}$:

$$\overline{\delta B} = \sqrt{\sum_{i=1}^{N}\left[\left(B_x - B_{m,x}\right)^2 + \left(B_y - B_{m,y}\right)^2 + \left(B_z - B_{m,z}\right)^2\right]/N}, \quad (2)$$

where N is the number of data points, to yield the parameters t_1 and t_2 for each range of magnetic activity (Table 1). Linear fits to t_1 and t_2 as a function of magnetic disturbance index were calculated (Figures 1b and 1c). We refer to Korth et al. (2015) for details of the fitting process. Higher cross-tail current intensities are seen for both the disk and the sheet current for higher magnetic activity. This result is consistent with the hypothesis that elevated magnetic activity leads to higher reconnection rates, stronger circulation of magnetic flux, and, ultimately, an increase in the strength of the cross-tail current.

A magnetic activity-dependent model of Mercury's magnetic field was developed by replacing the static values of the subsolar magnetopause standoff distance and the cross-tail current intensity parameters in the KT14 model with the linear dependencies on the magnetic disturbance index identified above. All other parameters remain identical to those listed in Korth et al. (2015). Figure 2 shows the magnetic field configurations of the revised model, termed KT17, for magnetic disturbance indices of 95% (black line) and 5% (blue dashed line) together with the average magnetopause (red line) for the 50% activity level. The tracing of magnetic fields lines shows a modest change in the size of the magnetosphere in response to variations in magnetic activity. The reference implementation of the KT17 model is included in the supporting information.

3. Discussion

The development of the KT17 model revealed new knowledge about Mercury's magnetosphere and also confirmed previously known characteristics. We confirmed the rigid shape of the magnetosphere, which on timescales of ~1 h (MESSENGER's average time inside the magnetosphere) is nearly invariant over a wide range of imposed solar wind and IMF conditions. At Earth, the standoff distance of the magnetopause at Earth has been observed to range from 10.7 ± 1.9 Earth radii (R_E) in response to variations of the solar wind pressure and from 10.9 ± 1.3 R_E in response to variations in IMF B_z (Sibeck et al., 1991). These variations correspond to deviations of R_{SS} from the mean of up to 18%. At Mercury, the R_{SS} range over the full range of magnetic activity is 1.42 ± 0.09 R_M (cf. Table 1). The maximum deviation of R_{SS} from the mean is only 6%, which is much less than observed at Earth. Comparison of the field lines for disturbance indices of 5% and 95% (Figure 2) further exhibits only small differences in the magnetotail diameter in response to a wide variation in external conditions. This result follows from the assumed self-similarity of the modeled magnetopause, consistent with the fitting of magnetopause crossings for disturbance indices ≤97%. Table 2 shows a decrease in the magnetotail radius, R_{Tail}, by about 0.3 R_M as the disturbance index increases from 10% to 90%, whereas the modeled magnetic field averaged over the lobe area, B_{Tail}, increases from ~18 nT to ~25 nT at a downtail distance of $X_{MSM} = -10\ R_M$. At this distance, all magnetic field lines are open, that is, they are connected to the planet in only one hemisphere, so that the magnetic flux connected to the polar cap in each hemisphere can be estimated from the lobe area and B_{Tail}. The modeled magnetic flux (Table 2) is 1.6 MWb on average and is somewhat lower than estimates (~2.6 MWb) obtained from observations (Johnson et al., 2012) because the KT17 model is fit to a globally distributed data set and matches the observations only in a least squares sense and because the flux was evaluated at a larger downtail distance. The result shows that the magnetic flux in the polar caps varies by only ~10% over almost the full range of magnetic activity and implies that, at Mercury, the polar cap size is nearly invariant and the magnetic energy stored in the magnetotail approximately

Table 2
Magnetotail Configuration at $X_{MSM} = -10\ R_M$ Sorted by Magnetic Disturbance

Disturbance index	$R_{Tail}\ (R_M)$	Lobe area (R_M^2)	B_{Tail} (nT)	Flux (MWb)
10	2.94	13.5	17.8	1.51
30	2.86	12.8	19.6	1.56
50	2.78	12.1	21.3	1.61
70	2.70	11.4	23.1	1.64
90	2.62	10.7	24.8	1.66

constant. This finding is consistent with the variations in the spatial extent of the large-scale Birkeland currents at Mercury (Anderson et al., 2014, Figure 2) and is in contrast to observations at Earth, where the polar cap expands in latitude by up to 15° equatorward (Anderson et al., 2017; Troshichev et al., 1996) as the magnetotail is loaded with magnetic flux in response to sudden enhancements of the dayside reconnection rate associated with increased geomagnetic activity. We note that, although Mercury's magnetosphere was found to be rigid and gently modulated over MESSENGER's magnetospheric transit time, the characteristics of Mercury's magnetosphere may deviate substantially on shorter timescales, for example, seconds to minutes. This was confirmed by observations of the instantaneous magnetopause position during individual MESSENGER transits into and out of the magnetosphere, which can deviate much more from the average position of this boundary. R_{SS} values inferred from individual magnetopause crossings range from less than 1 R_M (i.e., below the planetary surface) to ~2 R_M. These variations by up to a factor of 2 are much greater than those at Earth.

To test improvements in the model afforded by dynamic specification of parameters influenced by the highly variable solar wind conditions in Mercury's orbit, we computed the residuals between the observed magnetic field and that modeled using the associated magnetic disturbance index and heliocentric distance. The RMS value of these residuals is a measure of the goodness of the model, and a reduction thereof is an indicator of the improvement of the model. The overall RMS residual of the KT17 model computed using the entire set of data acquired between Mercury orbit insertion and the end of the mission using equation (2) is 25.3 nT and is slightly higher than the 24.8 nT reported for the KT14 model, which was fit to data acquired from orbit insertion to 28 November 2012 (Korth et al., 2015). The increase in the magnitude of the residual field may result from higher solar activity during the later orbital mission phase as indicated by a secondary maximum in the sunspot number in 2014 that was higher than that during the first peak in 2011. Consistent with this conjecture, the RMS residual of the KT14 model fit to the entire orbital data set is 26.5 nT, which is ~2 nT higher than the value reported by Korth et al. (2015) and that obtained for the KT17 model. Comparison of the misfit shows that the KT17 model yields only a minor reduction of the RMS residual corresponding to a very modest overall improvement in the model characterization of Mercury's magnetic field. The fact that the residual is lower for intervals that are less disturbed (Table 1) may indicate that magnetic activity is not fully accounted for in the KT17 model, presumably because magnetic activity changes faster than can be accounted for by the disturbance index computed on an orbit-by-orbit basis. However, as discussed further below, the largest contributions to the remaining residuals are likely from additional magnetic field sources not considered in the model.

To identify the source of the residuals, we computed the spatial distribution of the residuals. The spatial distribution was obtained by first sorting the residuals into bins of width 5° in latitude by 0.33 h in local time and then averaging the vector components in each bin. To first order, the distribution of the KT17 model residuals (Figures 3a–3c) is very similar to those obtained with the KT14 model (Korth et al., 2015, Figure 7). This finding is consistent with the modest differences of the RMS values of the magnetic residuals discussed above. To better locate the improvements of the dynamic model, we computed the variance reduction between the KT14 and KT17 models for each component of magnetic field in each latitude-longitude bin:

$$\Delta\sigma[\%] = \frac{\sum_{i=1}^{n} \delta B_{i,\mathrm{KT17}}^2 - \sum_{i=1}^{n} \delta B_{i,\mathrm{KT14}}^2}{\sum_{i=1}^{n} \delta B_{i,\mathrm{KT14}}^2} \cdot 100, \tag{3}$$

where $\delta B_{i,\mathrm{KT14}}$ and $\delta B_{i,\mathrm{KT17}}$ are residuals with respect to the KT14 and KT17 models, respectively, and n is the number of data points in a given latitude-longitude bin. The resulting distributions (Figures 3d–3f) show decreases in $\Delta\sigma$ for all magnetic field components in most spatial bins, demonstrating that the magnetic residuals are reduced over much of Mercury's magnetosphere sampled by the MESSENGER orbit. The largest reductions in the residuals were achieved near the dayside magnetopause, where most of the signal is in B_θ because the normal component of the magnetic field vanishes at the magnetopause by definition. Therefore, we attribute the reduction in the KT17 residuals on the dayside to improved modeling of the location and magnitude of magnetopause currents as function of magnetic activity. Increases in $\Delta\sigma$ are seen in only a few isolated locations near the dayside magnetopause and are likely related to errors in the identification of the magnetopause boundary crossing in the data. We note that the magnetic field
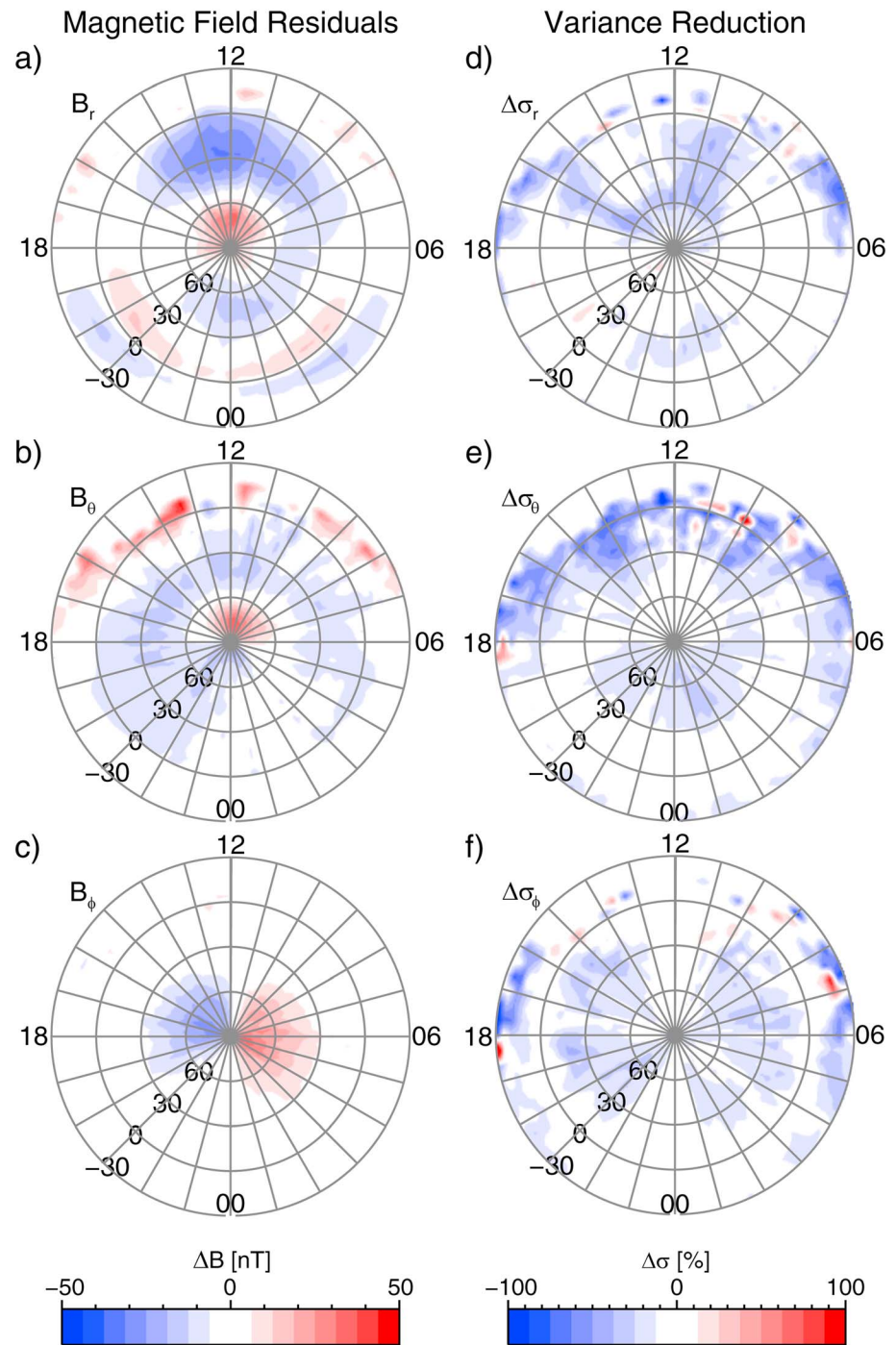
Figure 3. Mean residuals between the observed and modeled magnetic field for the (a) radial, B_r (positive outward); (b) colatitudinal, B_θ (positive southward); and (c) longitudinal, B_ϕ (positive eastward), components of a spherical coordinate system centered on the dipole. (d–f) The corresponding reduction in the component variances from the KT14 to KT17 models.

component normal to the magnetopause has been observed to deviate substantially from the model assumption that it be zero and may assume values up to 30% of the magnetic field intensity measured just inside the magnetopause (e.g., DiBraccio et al., 2013). Therefore, caution is advised when judging the goodness of the model near the dayside magnetopause using residuals in B_r. However, the reconnecting magnetic field component has only minor influence on the RMS residual because the latter is computed

from data measured throughout the magnetosphere of which data near the magnetopause resemble only a small fraction.

We have developed a dynamic model of Mercury's magnetospheric magnetic field and shown that, compared with a static model, magnetic residuals can be reduced by including magnetic activity in the parameterization of the model. The magnitudes of the binned RMS residuals between the observations and the KT17 model are typically well below 50 nT, and the model accounts for >90% of the internal and external magnetic fields in Mercury's magnetosphere. However, the large-scale distribution of residuals with respect to the static KT14 and dynamic KT17 models remains systematic and very similar. This result indicates that the primary cause of the magnetic residuals is likely not the result of magnetic activity and suggests that additional magnetospheric current sources not included in the model provide a moderate contribution to the magnetic field. One such source is the large-scale system of Birkeland currents (Birkeland, 1908), which flow along magnetic field lines between the magnetosphere and the planet at high latitudes. Their characteristic eastward (westward) magnetic field perturbations at dawn (dusk) have been discovered at Mercury (Anderson et al., 2014, 2017) and are evident in Figure 3c. The modular configuration of the KT17 model allows incorporation of contributions from Birkeland currents and other sources in the future. Further improvements are expected from increased spatial coverage of the observations as the two-spacecraft BepiColombo mission will continue Mercury's exploration in the mid-2020s.

References

Anderson, B. J., Johnson, C. L., & Korth, H. (2013). A magnetic disturbance index for Mercury's magnetic field derived from MESSENGER Magnetometer data. *Geochemistry, Geophysics, Geosystems*, 14, 3875–3886. https://doi.org/10.1002/ggge.20242

Anderson, B. J., Johnson, C. L., Korth, H., Slavin, J. A., Winslow, R. M., Phillips, R. J., … McNutt, R. L. Jr. (2014). Steady-state field-aligned currents at Mercury. *Geophysical Research Letters*, 41, 7444–7452. https://doi.org/10.1002/2014GL061677

Anderson, B. J., Johnson, C. L., Korth, H., Winslow, R. M., Borovsky, J. E., Purucker, M. E., … McNutt, R. L. Jr. (2012). Low-degree structure in Mercury's planetary magnetic field. *Journal of Geophysical Research*, 117, E00L12. https://doi.org/10.1029/2012JE004159

Anderson, B. J., Korth, H., Welling, D. T., Merkin, V. G., Wiltberger, M. J., Raeder, J., … Rastaetter, L. (2017). Comparison of predictive estimates of high-latitude electrodynamics with observations of global-scale Birkeland currents. *Space Weather*, 15, 352–373. https://doi.org/10.1002/2016SW001529

Birkeland, K. (1908). *The Norwegian Aurora Polaris Expedition, 1902–1903*. Oslo: H. Aschehoug.

Chapman, S., & Ferraro, V. C. A. (1931). A new theory of magnetic storms. *Terrestrial Magnetism*, 36, 171–186. https://doi.org/10.1029/TE036i003p00171

DiBraccio, G. A., Slavin, J. A., Boardsen, S. A., Anderson, B. J., Korth, H., Zurbuchen, T. H., … Solomon, S. C. (2013). MESSENGER observations of magnetopause structure and dynamics at Mercury. *Journal of Geophysical Research: Space Physics*, 118, 997–1008. https://doi.org/10.1002/jgra.50123

Dungey, J. W. (1963). Interactions of solar plasma with the geomagnetic field. *Planetary and Space Science*, 10, 233–237. https://doi.org/10.1016/0032-0633(63)90020-5

Johnson, C. L., Philpott, L. C., Anderson, B. J., Korth, H., Hauck, S. A., Heyner, D., … Solomon, S. C. (2016). MESSENGER observations of induced magnetic fields in Mercury's core. *Geophysical Research Letters*, 43, 2436–2444. https://doi.org/10.1002/2015GL067370

Johnson, C. L., Purucker, M. E., Korth, H., Anderson, B. J., Winslow, R. M., Al Asad, M. M. H., … Solomon, S. C. (2012). MESSENGER observations of Mercury's magnetic field structure. *Journal of Geophysical Research*, 117, E00L14. https://doi.org/10.1029/2012JE004217

Korth, H., Anderson, B. J., Acuña, M. H., Slavin, J. A., Tsyganenko, N. A., Solomon, S. C., & McNutt, R. L. Jr. (2004). Determination of the properties of Mercury's magnetic field by the MESSENGER mission. *Planetary and Space Science*, 52, 733–746. https://doi.org/10.1016/j.pss.2003.12.008

Korth, H., Anderson, B. J., Zurbuchen, T. H., Slavin, J. A., Perri, S., Boardsen, S. A., … McNutt, R. L. Jr. (2010). The interplanetary magnetic field environment at Mercury's orbit. *Planetary and Space Science*, 59, 2075–2085. https://doi.org/10.1016/j.pss.2010.10.014

Korth, H., Tsyganenko, N. A., Johnson, C. L., Philpott, L. C., Anderson, B. J., Al Asad, M. M., … McNutt, R. L. Jr. (2015). Modular model for Mercury's magnetospheric magnetic field confined within the average observed magnetopause. *Journal of Geophysical Research: Space Physics*, 120, 4503–4518. https://doi.org/10.1002/2015JA021022

Shue, J. H., Chao, J. K., Fu, H. C., Russell, C. T., Song, P., Khurana, K. K., & Singer, H. J. (1997). A new functional form to study the solar wind control of the magnetopause size and shape. *Journal of Geophysical Research*, 102, 9497–9511. https://doi.org/10.1029/97JA00196

Sibeck, D. G., Lopez, R. E., & Roelof, E. C. (1991). Solar-wind control of the magnetopause shape, location, and motion. *Journal of Geophysical Research*, 96, 5489–5495. https://doi.org/10.1029/90JA02464

Slavin, J. A., & Holzer, R. E. (1979). Effect of erosion on the solar wind stand-off distance at Mercury. *Journal of Geophysical Research*, 84, 2076–2082. https://doi.org/10.1029/JA084ia05p02076

Slavin, J. A., Acuña, M. H., Anderson, B. J., Baker, D. N., Benna, M., Boardsen, S. A., … Zurbuchen, T. H. (2009). MESSENGER observations of magnetic reconnection in Mercury's magnetosphere. *Science*, 324, 606–610. https://doi.org/10.1126/science.1172011

Slavin, J. A., Acuna, M. H., Anderson, B. J., Baker, D. N., Benna, M., Gloeckler, G., … Zurbuchen, T. H. (2008). Mercury's magnetosphere after MESSENGER's first flyby. *Science*, 321, 85–89. https://doi.org/10.1126/science.1159040

Slavin, J. A., Anderson, B. J., Baker, D. N., Benna, M., Boardsen, S. A., Gloeckler, G., … Zurbuchen, T. H. (2010). MESSENGER observations of extreme loading and unloading of Mercury's magnetic tail. *Science*, 329, 665–668. https://doi.org/10.1126/science.1188067

Slavin, J. A., DiBraccio, G. A., Gershman, D. J., Imber, S. M., Poh, G. K., Raines, J. M., … Solomon, S. C. (2014). MESSENGER observations of Mercury's dayside magnetosphere under extreme solar wind conditions. *Journal of Geophysical Research: Space Physics*, 119, 8087–8116. https://doi.org/10.1002/2014JA020319

Slavin, J. A., Imber, S. M., Boardsen, S. A., DiBraccio, G. A., Sundberg, T., Sarantos, M., … Solomon, S. C. (2012). MESSENGER observations of a flux-transfer-event shower at Mercury. *Journal of Geophysical Research*, 117, A00M06. https://doi.org/10.1029/2012JA017926

Slavin, J. A., Lepping, R. P., Wu, C. C., Anderson, B. J., Baker, D. N., Benna, M., … Zurbuchen, T. H. (2010). MESSENGER observations of large flux transfer events at Mercury. *Geophysical Research Letters*, *37*, L02105. https://doi.org/10.1029/2009GL041485

Solomon, S. C., McNutt, R. L. Jr., Gold, R. E., Acuna, M. H., Baker, D. N., Boynton, W. V., … Zuber, M. T. (2001). The MESSENGER mission to Mercury: Scientific objectives and implementation. *Planetary and Space Science*, *49*, 1445–1465. https://doi.org/10.1016/S0032-0633(01)00085-X

Sonnerup, B. U. (1974). Magnetopause reconnection rate. *Journal of Geophysical Research*, *79*, 1546–1549. https://doi.org/10.1029/JA079i010p01546

Spreiter, J. R., Summers, A. L., & Alksne, A. Y. (1966). Hydromagnetic flow around the magnetosphere. *Planetary and Space Science*, *14*, 223–253. https://doi.org/10.1016/0032-0633(66)90124-3

Troshichev, O., Hayakawa, H., Matsuoka, A., Mukai, T., & Tsuruda, K. (1996). Cross polar cap diameter and voltage as a function of PC index and interplanetary quantities. *Journal of Geophysical Research*, *101*, 13,429–13,435. https://doi.org/10.1029/95JA03672

Winslow, R. M., Anderson, B. J., Johnson, C. L., Slavin, J. A., Korth, H., Purucker, M. E., … Solomon, S. C. (2013). Mercury's magnetopause and bow shock from MESSENGER Magnetometer observations. *Journal of Geophysical Research: Space Physics*, *118*, 2213–2227. https://doi.org/10.1002/jgra.50237